

THE SPACE MOTION OF LEO I: THE MASS OF THE MILKY WAY'S DARK MATTER HALO

MICHAEL BOYLAN-KOLCHIN^{1,4,5}, JAMES S. BULLOCK¹, SANGMO TONY SOHN², GURTINA BESLA^{3,6},
& ROELAND P. VAN DER MAREL²

ApJ, in press

ABSTRACT

We combine our *Hubble Space Telescope* measurement of the proper motion of the Leo I dwarf spheroidal galaxy (presented in a companion paper) with the highest resolution numerical simulations of Galaxy-size dark matter halos in existence to constrain the mass of the Milky Way's dark matter halo ($M_{\text{vir,MW}}$). Despite Leo I's large Galacto-centric space velocity (200 km s^{-1}) and distance (261 kpc), we show that it is extremely unlikely to be unbound if Galactic satellites are associated with dark matter substructure, as 99.9% of subhalos in the simulations are bound to their host. The observed position and velocity of Leo I strongly disfavor a low mass Milky Way: if we assume that Leo I is the least bound of the Milky Way's classical satellites, then we find that $M_{\text{vir,MW}} > 10^{12} M_{\odot}$ at 95% confidence for a variety of Bayesian priors on $M_{\text{vir,MW}}$. In lower mass halos, it is vanishingly rare to find subhalos at 261 kpc moving as fast as Leo I. Should an additional classical satellite be found to be less bound than Leo I, this lower limit on $M_{\text{vir,MW}}$ would increase by 30%. Imposing a mass weighted Λ CDM prior, we find a median Milky Way virial mass of $M_{\text{vir,MW}} = 1.6 \times 10^{12} M_{\odot}$, with a 90% confidence interval of $[1.0 - 2.4] \times 10^{12} M_{\odot}$. We also confirm a strong correlation between subhalo infall time and orbital energy in the simulations and show that proper motions can aid significantly in interpreting the infall times and orbital histories of satellites.

Subject headings: galaxies: individual (Leo I) – Galaxy: kinematics and dynamics – Galaxy: halo – Galaxy: fundamental parameters – methods: N -body simulations

1. INTRODUCTION

Satellite galaxies orbiting the Milky Way (MW) have been a rich source of astrophysical information and cosmological confusion. Individually, these objects probe galaxy formation at the lowest masses, luminosities, and metallicities. As a population, the Milky Way's dwarf satellites offer one of the few existing tests of cosmology on small scales. They also provide a sample of tracers that can be used to estimate the mass distribution of the Milky Way's dark matter halo. Their small number, anisotropic spatial distribution, and unknown tangential velocities are all potential sources of biases and misunderstandings, however.

In particular, Leo I has long been known to play an outsized role when using satellite galaxies to determine the mass of the Milky Way's dark matter halo ($M_{\text{vir,MW}}$; Zaritsky et al. 1989; Fich & Tremaine 1991; Kochanek 1996) because of its large distance and high radial velocity in the Galacto-centric frame. In the analysis of Watkins et al. (2010), which incorporates line-of-sight velocity information for 25 Galactic satellites in determining $M_{\text{vir,MW}}$, Leo I alone contributes approximately 27% to the mass estimate (i.e., including Leo I leads to mass estimates that are 25-30% larger than those that

exclude Leo I).

Incorporating Leo I into an estimate of $M_{\text{vir,MW}}$ generally requires the assumption that Leo I is indeed bound. The timing argument (Kahn & Woltjer 1959), for example, assumes the MW and Leo I to be on an elliptical orbit, with Leo I having made a recent pericentric pass about the Milky Way. Since Leo I is, by assumption, bound to the Milky Way in such analyses, a large Milky Way mass is required to match Leo I's observed distance and radial velocity (e.g., Zaritsky et al. 1989; Li & White 2008; Sohn et al. 2012b). If Leo I is unbound, however, the timing argument as applied to Leo I will almost certainly overestimate $M_{\text{vir,MW}}$. Leo I's extreme kinematic properties have therefore led to substantial debate about its status as a bound satellite of the Milky Way (Zaritsky et al. 1989; Byrd et al. 1994; Sales et al. 2007; Sohn et al. 2007; Mateo et al. 2008).

Theoretical models of halo collapse provide a further basis for interpreting satellite orbits in Λ CDM. In particular, the self-similar secondary infall model (SSIM; Fillmore & Goldreich 1984; Bertschinger 1985) has guided much of the progress in understanding halo collapse and virialization. In the simplest version of the SSIM – one where only radial motions are considered – the matter flow around a slight overdensity in the early universe can be derived in a straightforward manner. Shells of matter around the overdensity initially expand with the Hubble flow. Those shells that are bound to the perturbation eventually reach a turn-around radius and re-collapse, with more bound shells collapsing earlier; the virial radius of a halo is approximately equal to half of the present day turn-around radius in the SSIM. In this model, then, *all* accreted material must be bound; otherwise, it would

¹ Center for Cosmology, Department of Physics and Astronomy, 4129 Reines Hall, University of California, Irvine, CA 92697, USA

² Space Telescope Science Institute, 3700 San Martin Drive, Baltimore, MD 21218, USA

³ Department of Astronomy, Columbia University, New York, NY 10027, USA

⁴ email: m.bk@uci.edu

⁵ Center for Galaxy Evolution fellow

⁶ Hubble fellow

not collapse onto the overdensity.

Although the physical picture of accretion in a hierarchical universe is somewhat different from the smooth SSIM, analyses of N -body simulations have shown that phase space is often structured in a very similar manner to SSIM predictions (e.g., [Ascasibar et al. 2007](#); [Diemand & Kuhlen 2008](#)). With numerical simulations, it is possible to compute the orbits of halos falling into larger halos. Studies of large volume cosmological simulations generally find that unbound orbits are very rare, in accordance with the expectations of the SSIM: [Wetzel \(2011\)](#) found that less than 2% of orbits are unbound at all redshifts, while [Benson \(2005\)](#) found that only 0.3% of all orbits escape the host halo. These analyses typically adopt the point mass limit and therefore underestimate the potential energy of the orbit coming from the mass distribution exterior to the halos; accordingly, these unbound fractions should be upper limits to the true unbound fraction. While the works of Benson and Wetzel studied orbits of merging dark matter satellites across a broad spectrum of dark matter halo masses, [Deason et al. \(2011\)](#) and [Di Cintio et al. \(2012\)](#) focused on Milky Way-mass systems, again finding that the fraction of unbound satellites is quite low. In this paper, we show that the eight highest resolution simulations performed to date of Milky Way-size halos all have unbound fractions of less than 1 in 1000 (0.1%).

In accordance with predictions of the SSIM, N -body simulations show that halos falling into larger halos have a characteristic orbital energy that is roughly invariant with time: for host halos with $M_{\text{vir}} \sim 10^{12} M_{\odot}$, this energy corresponds to an orbital velocity of $\approx 1.1 V_{\text{vir}}$ at the virial radius, with a 1σ scatter of 25% ([Wetzel 2011](#); see also [Benson 2005](#); [Khochfar & Burkert 2006](#)). Since halo virial masses grow with time, due to physical mass accretion or to a time-varying virial overdensity threshold ([Diemand et al. 2007b](#); [Diemer et al. 2012](#)), subhalos accreted at early times will be somewhat more tightly bound than those accreted more recently. Once an infalling halo has interacted substantially with the host, its orbital energy may decrease owing to processes such as dynamical friction; much less frequently, it may gain orbital energy through three-body interactions. Fluctuations in the central gravitational potential of the host due to, e.g., virialization or mergers may also affect subhalos' energies. Subhalos that have been part of their host for a long time will therefore exhibit a wide range of orbital energies, whereas recently accreted subhalos should occupy a much narrower range in energy space (and should be less strongly bound).

This general picture has been confirmed by [Diemand & Kuhlen \(2008\)](#), who show a strong relationship between the number of orbits a subhalo has completed and its position in radial velocity phase space for the Via Lactea (VL) simulation ([Diemand et al. 2007a](#)), and by [Rocha et al. \(2012\)](#), who found a clear correlation between orbital binding energy and infall time for subhalos in the Via Lactea II simulation (VL-II; [Diemand et al. 2008](#)). Similar relationships are generically expected in the SSIM, although this model does not account for energy loss processes such as dynamical friction. Note that both in the SSIM and in cosmological simulations, satellites falling into dark matter halos for the first time do so on bound orbits: *a first infall need not, and almost*

always does not, imply an unbound orbit.

The three-body interactions discussed in the previous paragraphs provide a means of boosting the velocities of some subhalos to above the local escape velocity, however. This possibility has received attention in the literature recently, often in the context of exploring “extreme” objects such as Leo I. [Sales et al. \(2007\)](#) emphasized the existence of dark matter satellites that have gained energy through three-body interactions with other, more massive satellites inside of their host halos. [Ludlow et al. \(2009\)](#) examined subhalo orbits around Milky Way halos as well and showed that many satellites travel to large apocentric distances, much larger than would be expected from their initial orbits, after gaining energy through the aforementioned three-body interactions during their first pericentric pass. Even after gaining energy, these satellites typically remain formally bound to their dark matter host, although their apocenters can (significantly) exceed their original turn-around radius. These “ejected” subhalos always have very low mass at infall (0.1% of their host’s mass or less; [Ludlow et al. 2009](#)) and are usually found as the companion of a more massive infalling satellite ([Sales et al. 2007](#)). An additional phenomenon specific to the environments around pairs of similarly massive halos, such as the Local Group, is that of “renegade” satellites ([Knebe et al. 2011](#); [Teyssier et al. 2012](#)), which are objects presently near one halo but that were, at some earlier epoch, within the virialized extent of the other halo.

Although a variety of complicated orbital histories are possible for subhalos, such orbits constitute a small minority of the satellite population around dark matter halos. Most subhalos at large distances (1 – 2 virial radii) from their hosts have not undergone any complex interactions with multiple other bodies. Analytic models predict, and Λ CDM simulations find, that many satellites once well within a host’s virial radius will spend significant time at larger radii ([Mamon et al. 2004](#); [Gill et al. 2005](#); [Wang et al. 2009](#)), a natural consequence of the highly eccentric nature of subhalo orbits (the median apocenter to pericenter distance ratio for subhalos is approximately 6:1; [Ghigna et al. 1998](#); [Diemand et al. 2007b](#)). Distant MW satellites such as Leo I may well fall into this class of objects.

While the uncertainty surrounding Leo I’s status as a bound MW satellite is a source of frustration, this does not diminish the importance of Leo I in establishing the dark matter distribution around the Milky Way. There are few kinematic tracers for $D \gtrsim 80$ kpc (see, e.g., [Gnedin et al. 2010](#); [Deason et al. 2012](#)), and deriving mass constraints from these tracers (typically blue horizontal branch stars) requires assumptions about their spatial distribution and velocity anisotropies ([Dehnen et al. 2006](#); [Deason et al. 2012](#)).

In a companion paper ([Sohn et al. 2012b](#); hereafter, Paper I), we presented the first determination of Leo I’s transverse velocity, based on proper motion measurements using the unique astrometric capabilities of the *Hubble Space Telescope (HST)*. This provides a direct probe of the mass distribution of the Milky Way at 260 kpc, where the potential is dominated by the dark matter halo, and therefore a new window on $M_{\text{vir,MW}}$. In this paper, we combine the measurement of the proper motion of Leo I from Paper I with state-of-the-art numerical

simulations of the formation of Milky Way-size halos in Λ CDM in order to constrain the mass of the Galaxy’s dark matter halo.

There is considerable disagreement in the existing literature about $M_{\text{vir,MW}}$. Direct measures have typically focused on tracers of the inner portions of the Milky Way’s dark matter halo ($d \lesssim 80$ kpc) based on measured velocities of giant stars, with recent results ranging from $\sim [0.8 - 1.0] \times 10^{12} M_{\odot}$ (Battaglia et al. 2005; Xue et al. 2008) to $1.6 \times 10^{12} M_{\odot}$ (Gnedin et al. 2010). Most recently, Deason et al. (2012) argued that the mass of the halo within 150 kpc likely falls in the range of $[0.5 - 1.0] \times 10^{12} M_{\odot}$. Using radial velocities of nearby stars from the RAVE survey to compute the local escape velocity, Smith et al. (2007) estimated that $M_{\text{vir,MW}} = 0.85 \times 10^{12} M_{\odot}$ for a standard NFW halo, or $1.42 \times 10^{12} M_{\odot}$ for an adiabatically contracted dark matter halo.

Published measurements using the radial velocities of satellite galaxies give an even wider range, from $\sim [0.8 - 2.5] \times 10^{12} M_{\odot}$, depending on the satellites included and assumptions about the orbits of those satellites (Kochanek 1996; Watkins et al. 2010). Boylan-Kolchin et al. (2011a) and Buscha et al. (2011) combined analyses of large N -body simulations with the Kallivayalil et al. (2006b) measurement of the Large Magellanic Cloud’s proper motion and obtained $M_{\text{vir,MW}} \approx 2 \times 10^{12}$ and $1.2 \times 10^{12} M_{\odot}$, respectively. Previous determinations of $M_{\text{vir,MW}}$ based on the Leo I timing argument have ranged from $[1 - 3] \times 10^{12} M_{\odot}$ (Zaritsky et al. 1989; Kochanek 1996; Li & White 2008, Paper I), while the Milky Way-M31 timing argument is also more consistent with values of $M_{\text{vir,MW}}$ that are somewhat higher than those obtained via stellar tracers (van der Marel et al. 2012b).

Indirect constraints on $M_{\text{vir,MW}}$ can be obtained from combinations of galaxy-galaxy lensing and Tully-Fisher data. Dutton et al. (2010) and Reyes et al. (2011) parameterize this combination of data in terms of the typical ratio of a galaxy’s optical velocity V_{opt} (the circular velocity at 2.2 disk scale radii) to its virial velocity⁷ V_{200c} . Reyes et al. find $V_{\text{opt}} = 1.27 V_{200c}$ for galaxies with stellar masses equal to that of the Milky Way ($M_{\star,\text{MW}} \approx 6 \times 10^{10} M_{\odot}$; Flynn et al. 2006; McMillan 2011); including scatter in concentration at fixed mass, this becomes $V_{\text{opt}} < 1.8 V_{200c}$ (2σ). Using $V_{\text{opt,MW}} = 240 \text{ km s}^{-1}$ (McMillan 2011; Schönrich 2012), we find that Reyes et al. predict a median value of $M_{\text{vir,MW}} \approx 2.5 \times 10^{12} M_{\odot}$, with $M_{\text{vir,MW}} \gtrsim 1.16 \times 10^{12} M_{\odot}$ (2σ). This is similar to abundance matching’s prediction of $M_{\text{vir,MW}} \approx 2.5 \times 10^{12} M_{\odot}$ for this stellar mass (Guo et al. 2010; Reddick et al. 2012; Moster et al. 2013).

In light of these results, it is fair to say that the mass of the Milky Way is known to no better than a factor of two, and possibly even worse; indeed, Klypin et al. (2002) showed that a wide range of observational data can be fit both for $M_{\text{vir}} = 10^{12}$ and for 2×10^{12} . This uncertainty is a fundamental limitation in understanding several pressing questions related to galaxy formation and cosmology.

⁷ These authors define the virial velocity to be the halo’s circular velocity at the radius containing an average density of 200 times the critical density.

For example, it is frequently assumed that galaxies have available to them $(\Omega_b/\Omega_m) \times M_{\text{vir}}$ in baryons. If $M_{\text{vir,MW}} = 5 \times 10^{11} M_{\odot}$, then essentially all of those baryons are accounted for by observed stars and gas in and around the Galaxy; if $M_{\text{vir,MW}} = 2.5 \times 10^{12} M_{\odot}$, then a large majority of the Milky Way’s baryons are missing (Fukugita & Peebles 2004; Anderson & Bregman 2010; Gupta et al. 2012; Fang et al. 2013). Another example is the predicted abundance of dark matter satellites, which scales nearly linearly with dark matter halo mass; the expected mass of a galaxy’s most massive satellite scales in the same manner. As a result, our interpretation of the missing satellites problem (Klypin et al. 1999; Moore et al. 1999) and related questions about the Galaxy’s satellite population depends on $M_{\text{vir,MW}}$ (Boylan-Kolchin et al. 2011b, 2012; Wang et al. 2012; Vera-Ciro et al. 2013).

A measurement of the mass distribution of the Milky Way at large Galacto-centric distance ($D > 100$ kpc) would bring significantly more clarity to each of these issues. Here, we use the results of Paper I in conjunction with cosmological simulations of Milky Way-size dark matter halos to provide a constraint on $M_{\text{vir,MW}}$ based on the proper motion of Leo I ($D = 260.6$ kpc). This paper is structured as follows. Section 2 describes the simulations we employ and provides a summary of the results of Paper I. We then compare the simulations to the radial velocity (Section 3.1) and space velocity (Section 3.2) of Leo I. This allows us to constrain the Milky Way’s virial mass (Section 4). We discuss our results in the context of expected infall times of Λ CDM satellites in general, and Leo I in particular, in Section 5, and conclude with a brief summary and discussion of our results in Section 6.

2. SIMULATIONS AND DATA

2.1. Simulations

Our primary set of Milky Way-size halos are those of the Aquarius simulation (Springel et al. 2008a). The simulations, and the properties of the halos, have been extensively discussed elsewhere (e.g., Springel et al. 2008a,b; Navarro et al. 2010), and we refer the reader to those papers for details related to the simulations. We use the six halos (denoted A-F) simulated at “level two” resolution of $\approx 10^4 M_{\odot}$ per particle with Plummer-equivalent gravitational softening length of 66 pc. The Aquarius suite was run assuming a WMAP-1 cosmology with parameters $\Omega_m = 0.25$, $\Omega_{\Lambda} = 0.75$, $\sigma_8 = 0.9$, $H_0 = 73 \text{ km s}^{-1} \text{ Mpc}^{-1}$, $n_s = 1.0$. More recent measurements prefer slightly different values of these parameters, but these differences are not expected to affect the assembly and internal dynamics of Milky Way-mass halos at a substantive level and are therefore unimportant for our analysis. In Appendix A, we compare results from similarly well-resolved halos – VL-II and GHALO (Stadel et al. 2009) – using WMAP3 parameters to show this explicitly.

The virial mass M_{vir} of a dark matter halo is not uniquely defined, but rather depends on the density threshold used to define a dark matter halo. Throughout this work, we will define M_{vir} to be the mass within a sphere, centered on the halo in question, containing an average density Δ times the critical density of the Uni-

verse; we use $\Delta = \Delta_{\text{vir}}$, the value derived from the spherical top-hat collapse model (Gunn & Gott 1972; Bryan & Norman 1998), which gives $\Delta_{\text{vir}} \approx 94$ at $z = 0$ for the cosmology of the Aquarius simulations. Note that other common choices of Δ are 200 and $200\Omega_m(z)$. The Aquarius halos have $0.95 < M_{\text{vir}}/10^{12} M_{\odot} < 2.2$, which is a reasonable approximation of current constraints on the value of the Milky Way’s virial mass (see Boylan-Kolchin et al. 2012 for a recent compilation).

In the Λ CDM cosmogony, all satellite galaxies are expected to initially form within their own dark matter halo, outside of their host’s virial radius. The luminous satellite galaxies of the Milky Way are therefore expected to be represented by some subset of dark matter subhalos surviving to $z = 0$. The precise relationship between satellite galaxies and dark matter subhalos is presently unclear; however, all models of galaxy formation predict a good correspondence between the most luminous satellite galaxies and the most massive subhalos for some suitable definition of mass, most often the maximum mass or circular velocity that the subhalo has ever had (e.g., Kravtsov et al. 2004; Conroy et al. 2006; Guo et al. 2010; Yang et al. 2012; Reddick et al. 2012; Behroozi et al. 2012; Moster et al. 2013). We therefore record the redshift at which a subhalo’s bound mass is maximized, which we hereafter refer to as the infall redshift⁸ z_{infall} , as well as the maximum circular velocity at that time, V_{infall} .

Dark matter subhalos with maximum circular velocities in excess of 5 km s^{-1} and having $V_{\text{max}} > 0.044 V_{\text{vir}}$ (corresponding to 5 km s^{-1} for the lowest mass halo, Aq-B) are selected for further analysis. All halos and subhalos satisfying this V_{max} threshold within one Megaparsec of each Aquarius main halo are considered, with no additional velocity-based criteria. This ensures we do not introduce any bias against high velocity objects in our analysis. All distances and velocities discussed below are computed in the halo-centric frame.

2.2. Observational Data

The observational data used in our analysis are detailed in Paper I. For the purposes of this work, the important quantities are as follows.

- The Galacto-centric distance to Leo I (D_{LeoI}):

$$D_{\text{LeoI}} = 260.6 \pm 13.3 \text{ kpc} \quad (1)$$

- The Galacto-centric radial velocity of Leo I ($V_{r,\text{LeoI}}$):

$$V_{r,\text{LeoI}} = 167.9 \pm 2.8 \text{ km s}^{-1} \quad (2)$$

- The Galacto-centric transverse (tangential) velocity of Leo I ($V_{t,\text{LeoI}}$):

$$V_{t,\text{LeoI}} = 101.0 \pm 34.4 \text{ km s}^{-1}. \quad (3)$$

The measured three-dimensional Galacto-centric space velocity of Leo I is

$$V_{\text{LeoI}} = 199.8_{-17.2(-29.3)}^{+21.8(+47.0)} \text{ km s}^{-1}, \quad (4)$$

⁸ This definition of infall time is similar to the time a subhalo last crossed the physical boundary of its host but does not rely on any specific definition of the host’s “edge”.

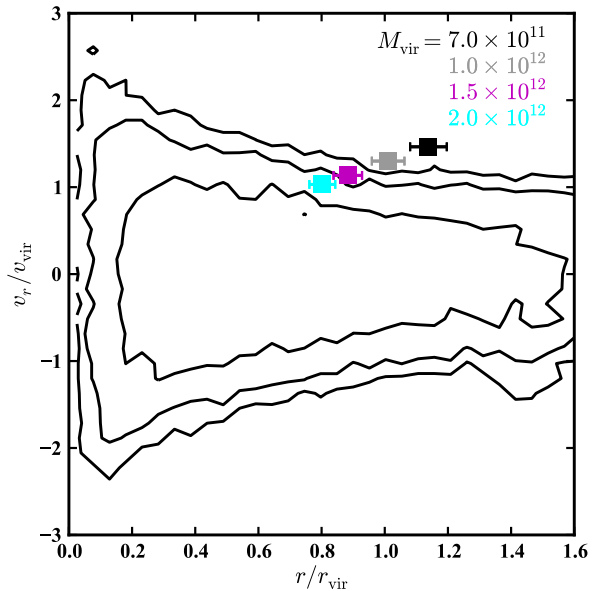


FIG. 1.— Radial phase space diagram of Aquarius subhalos, scaled to virial units. The inner, middle, and outer contours contain 68, 95.4, and 99.7% of subhalos from the Aquarius simulations. Colored squares with error bars show the location in phase space of Leo I, with 1σ uncertainties, for a variety of assumed virial masses for the Milky Way. Note that the absolute error on the radial velocity is smaller than the size of the symbols. The observed values of (r, v_r) for Leo I are consistent with fewer than 0.3% of the Aquarius subhalos if the MW virial mass is less than $1.1 \times 10^{12} M_{\odot}$.

where the errors – computed from Monte Carlo sampling of the proper motion error space – represent 68.27% (95.45%) confidence intervals about the stated median.

3. INTERPRETING THE MOTION OF LEO I

3.1. The radial velocity of Leo I

Figure 1 shows a phase space diagram for all subhalos in the Aquarius simulations. The radial velocity V_r of each subhalo is scaled by the virial velocity of its host, and the halo-centric radius of each subhalo is likewise scaled by the virial radius of the host. Infalling subhalos have $V_r < 0$, while outgoing subhalos have positive radial velocities. The black contours contain 68.3%, 95.5%, and 99.7% of subhalos⁹. Additionally, we have placed square symbols with error bars¹⁰ on the plot to denote the observed position of Leo I in this phase space for four representative values of the Milky Way’s virial mass: $M_{\text{vir,MW}}/10^{12} M_{\odot} = 0.7$ (black), 1.0 (gray), 1.5 (magenta), and 2.0 (cyan).

It is obvious why the observed radial velocity of Leo I has demanded a high virial mass for the Milky Way: subhalos in both the 7×10^{11} and $10^{12} M_{\odot}$ halos have radial velocities as high as Leo I less than 0.3% of the time. In more massive halos, Leo I’s high radial velocity becomes more likely; however, it is still higher than 70% of subhalos at Leo I’s Galacto-centric distance in a halo with $M_{\text{vir}} = 2 \times 10^{12} M_{\odot}$. With only a measurement of Leo I’s radial velocity, the preferred mass of the MW is significantly in excess of $10^{12} M_{\odot}$. Constraining M_{vir}

⁹ The contour value at a specific radius for a given percentage value is computed by finding the location of that value in the cumulative distribution function of V_r at that radius.

¹⁰ Unless otherwise noted, all plotted error bars are 1σ .

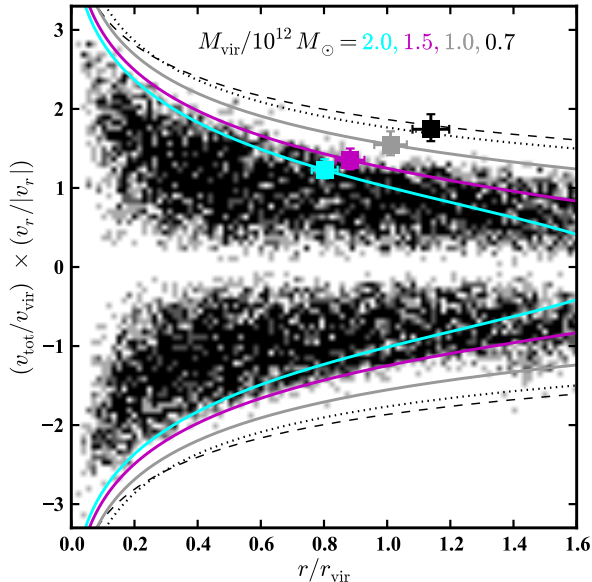


FIG. 2.— The phase space diagram for Aquarius subhalos using their space velocity; velocities and positions are scaled by virial values. At each radius, the velocity distribution is roughly Maxwellian rather than Gaussian; the distributions are maximized near $V_{\text{tot}} \approx V_{\text{vir}}$ for a wide range of radii. The colored squares show Leo I’s location in this phase space, using the measurement of V_t from Paper I, for representative values of $M_{\text{vir,MW}}$ (the colors are the same as in Fig. 1). Colored lines show surfaces of constant energy in an NFW potential, while the dashed (dotted) curve shows the escape velocity for an NFW potential with a concentration of 8 (16). For virial masses less than $\approx 1.2 \times 10^{12} M_{\odot}$, Leo I is less bound than virtually all Aquarius subhalos.

more tightly requires knowledge of the transverse velocity of Leo I, however, as it requires understanding how likely it is for a subhalo to be on an unbound orbit about its host, and whether the observed tangential velocity of Leo I is cosmologically plausible, given its radial velocity. Furthermore, as we demonstrate in Section 5, satellites that have been recently accreted occupy a wide range of radial velocities but are confined to a much narrower range of total velocities. In combination with reasonable estimates of infall times (based on, e.g., star formation histories), 3D velocity information can therefore be much more constraining than radial velocity information alone.

3.2. The space velocity of Leo I

The analysis of section 3.1 does not require any knowledge of the transverse velocity of Leo I. In this section, we incorporate the measurement of $V_{t,\text{LeoI}}$ from Paper I to compare the full space velocity of Leo I to simulated Λ CDM satellites. In Figure 2, we again plot the phase space diagram of Aquarius subhalos, this time using total velocity V rather than radial velocity on the vertical axis. The direction of the radial velocity of each satellite is indicated by the sign of the total velocity: negative (positive) for inward (outward) radial velocities.

We place Leo I on the plot for the same four choices of the Milky Way’s virial mass used in Figure 1: $M_{\text{vir,MW}}/10^{12} M_{\odot} = 0.7$ (black), 1.0 (gray), 1.5 (magenta), and 2.0 (cyan). Lines of constant energy for an object with Leo I’s Galacto-centric distance and observed velocity for each of these halo masses are also plotted using the same color scheme, assuming a dark matter halo following a Navarro, Frenk, & White (1997, hereafter

NFW) profile with a concentration of $c = 12$ (Macciò et al. 2007). Also plotted in Figure 2 are curves corresponding to the escape velocity V_{esc} as a function of radius for an NFW profile with a concentration parameter of 8 (black dashed curve) and 16 (black dotted curve), assuming the NFW profile is infinite in extent. Note that while the mass of such a profile is logarithmically divergent with radius, the gravitational potential is finite at all radii and the escape velocity is well-defined. In this representation, these curves are independent of the assumed halo mass. The values used ($c = 8, 16$) approximately span the expected 1σ scatter in concentration at fixed mass for Milky Way-size halos (Bullock et al. 2001; Macciò et al. 2007; Boylan-Kolchin et al. 2010; Klypin et al. 2011).

A remarkable feature of Fig. 2 is that vanishingly few subhalos – to be precise, only one in our entire Aquarius sample, or 0.01% – have orbits that are unbound ($V > V_{\text{esc}}$). Furthermore, this single unbound subhalo is part of a massive ($M_{\text{vir}} \approx 1.3 \times 10^{11} M_{\odot}$) infalling group¹¹ at $r \approx 1.4 r_{\text{vir}}$ in the Aquarius C halo, and is therefore a somewhat special case. Similar results are found for VL-II (0.06 % unbound) and GHALO (no unbound subhalos); see the Appendix for a version of Fig 2 that includes VL-II and GHALO data.

All eight of these high-resolution simulations target individual Milky Way-size dark matter halos, while the Milky Way has a close neighbor of comparable mass, M31. In order to assess possible effects of Local Group-like environments on the unbound fraction of dark matter subhalos, we also have analyzed a series of Local Group simulations from the ELVIS project (Garrison-Kimmel et al., in preparation), which includes a suite of dark matter re-simulations of Local Group analogs in the WMAP 7 cosmology. The vast majority of ELVIS halos have no unbound subhalos, in agreement with the Aquarius, VL-II, and GHALO results. The $\sim 1\%$ unbound fraction in the other ELVIS halos are either (1) the result of very recent major mergers, or (2) subhalos associated with a massive, recently-accreted object. The first situation is not relevant for the Milky Way, while the orbit integrations in Paper I demonstrate that the second situation is not applicable to Leo I. The same calculations further show that Leo I has not interacted with Andromeda over the past Hubble time, indicating that M31 has not been a major dynamical influence on Leo I’s orbit.

The negligible unbound fractions found in the ELVIS resimulations appear to be in conflict with results from the CLUES project,¹² which consists of a number of constrained simulations of the Local Group: Di Cintio et al. (2012) found that approximately 3% of subhalos within r_{vir} are unbound in the CLUES Local Group analogs. This difference, however, has its origin in how escape velocities are computed in our analysis and in Di Cintio et al. (2012), not in the properties of the simulations themselves. The Amiga Halo Finder (Knollmann & Knebe 2009), which was used for identifying subhalos in the CLUES runs, calculates the gravitational potential of a halo by assuming that it is truncated at r_{vir} . Allowing for the mass external to r_{vir} , as in our calcula-

¹¹ This group can be seen as a deformation of the contours at $v_r \approx -1.5 V_{\text{vir}}$ in Figure 1

¹² <http://www.clues-project.org/index.html>

tions, results in larger binding energies and significantly reduces the unbound fraction. As an example, an NFW profile with $M_{\text{vir}} = 7 \times 10^{11}$ and $c = 8$ places Leo I on a parabolic orbit ($V_{\text{esc}} = V_{\text{LeoI}}$), whereas the same mass distribution, truncated at D_{LeoI} , has an escape velocity that is 20% lower, $\sim 160 \text{ km s}^{-1}$. The difference between extended and truncated mass distributions is even more pronounced for higher values of M_{vir} .

We have explicitly checked that the unbound fractions in Aquarius, VL-II, and GHALO are comparable to those from Di Cintio et al. (2012) if we artificially truncate the mass distribution at r_{vir} . We therefore conclude that our calculations regarding the very low unbound fractions in Milky Way-sized halos are likely robust to the presence or absence of an Andromeda analog, so long as the full mass distribution surrounding the halo(s) is considered. The precise unbound fraction clearly depends on the specific definition of the truncation radius of the gravitational potential – or, equivalently, on the potential’s zero point. The constraints on the virial mass of the Milky Way that we derive in Section 4 do not depend on whether Leo I is unbound in an absolute sense (which is an ill-posed question in a cosmological context), but only on how bound it is relative to other Milky Way satellites and to subhalos in N -body simulations; these quantities are independent of the choice of truncation radius.

Based on our analysis of the eight highest resolution Λ CDM N -body simulations of Milky Way-sized dark matter halos performed to date, it is very unlikely that Leo I is on an unbound orbit. This point is also consistent with both theoretical models of halo formation and numerical simulations of structure formation, as discussed in the Introduction¹³. Although unbound orbits are quite rare in the simulations adopted here, they are fully incorporated in our analysis. Likewise, our analysis already includes any subhalos with energies that have been boosted by three-body interactions. That Leo I is almost certainly bound imposes a weak constraint on the MW mass in the context of Λ CDM, however: this requires only that $M_{\text{vir,MW}} \gtrsim 0.7 \times 10^{12} M_{\odot}$ (ignoring proper motion errors). In the next section, we combine the proper motion results of Paper I with the Aquarius subhalo data introduced above to derive more stringent lower limits on the virial mass of the Milky Way.

4. CONSTRAINING THE MILKY WAY’S VIRIAL MASS

While the Aquarius halos provide us with a large sample of subhalos, the host halos themselves only give us six different virial masses. The results of Figures 2 and 7 indicate that halos in the mass range of interest for the Milky Way are very close to self-similar in terms of the kinematics of their subhalo populations, however, when each halo is scaled to virial quantities. We can therefore use our Aquarius sample to interpret Leo I’s motion in a variety of halo masses. In practice, this simply means that to change from a halo with original virial quantities (M, R, V) to a halo with virial quantities (M', R', V'), we multiply all radii by R'/R and all velocities by V'/V .

Given a subhalo’s current position and velocity, we compute the velocity it would have at the Galactocentric

distance of Leo I based on its binding energy. The orbital energy of a subhalo is calculated using a spherically symmetric NFW profile with $c = 12$. We have compared this calculation to using the full gravitational potential computed from the parent N -body simulation and find very good agreement, with a small level ($< 10\%$) of symmetric scatter at a given radius due to non-sphericity of the gravitational potential (see, e.g., Hayashi et al. 2007).

The probability that a random subhalo i has a binding energy \mathcal{E} less than that of Leo I (i.e., that the subhalo is less bound than Leo I) – $p(\mathcal{E}_i < \mathcal{E}_{\text{LeoI}})$ – is then equal to the probability of subhalo i having a space velocity greater than that of Leo I. We incorporate the Monte Carlo samplings of the proper motion error space described in Paper I when computing $p_i = p(\mathcal{E}_i < \mathcal{E}_{\text{LeoI}})$. For an ensemble of N subhalos, the probability that one subhalo chosen at random is less bound than Leo I is

$$P(\mathcal{E} < \mathcal{E}_{\text{LeoI}}) = \frac{1}{N} \sum_i p_i. \quad (5)$$

We consider only satellites with positive radial velocities (subhalos moving away from the halo center, as is the case for Leo I) in our analysis in order to make a fair comparison to the dynamics of Leo I.

The left panel of Figure 3 shows probability distributions for finding subhalos on orbits at least as energetic as that of Leo I. The dotted curve shows the result when considering any individual galaxy. Even at $M_{\text{vir}} = 2 \times 10^{12} M_{\odot}$, a randomly selected subhalo only has a 20% chance of being less bound than Leo I. Of course, part of the motivation for obtaining measurements of Leo I’s proper motion was its high radial velocity, i.e., Leo I is *not* a randomly chosen satellite. The probability of finding a high velocity satellite will obviously increase as the sample size of satellites increases.

Ideally, we would use proper motion data for a statistically representative set of satellite galaxies. Unfortunately, only five Milky Way satellites have measured space velocities that are accurate at the 25% level¹⁴. This is still a data set without an obvious, homogeneous selection function, although we note it does consist of the five most luminous Milky Way satellites (excluding the Sagittarius dwarf spheroidal). A blind search for Galactic satellites, irrespective of luminosity, will preferentially find nearby satellites owing to luminosity bias. This bias does not affect searches within $\sim 400 \text{ kpc}$ of the Milky Way for satellites with $L_V \gtrsim 10^5 L_{\odot}$, so long as there is not a population of very extended satellites above this luminosity with surface brightnesses that fall below current detection limits. The 11 “classical” satellites of the Milky Way (e.g., Mateo 1998) therefore comprise a sample with a relatively well-known selection function. We can then ask how likely it is to find a satellite on an orbit as energetic as Leo I’s when selecting from a sample of this size. Note that this should result in lower limits for the MW mass that are conservative (in the sense that different assumptions about the unknown transverse velocities of six classical satellites will only lead to an increased lower limit on $M_{\text{vir,MW}}$), as fewer than half of these 11 satellites have measured space velocities.

¹³ The same logic can be applied to fast-moving satellites of M31, such as And XII and XIV (McConnachie 2012), meaning they are also likely to be bound satellites.

¹⁴ These satellites are the Large and Small Magellanic Clouds (Kallivayalil et al. 2006b,a; Piatek et al. 2008), Fornax (Piatek et al. 2007), Sculptor (Piatek et al. 2006), and Leo I (Sohn et al. 2012b).

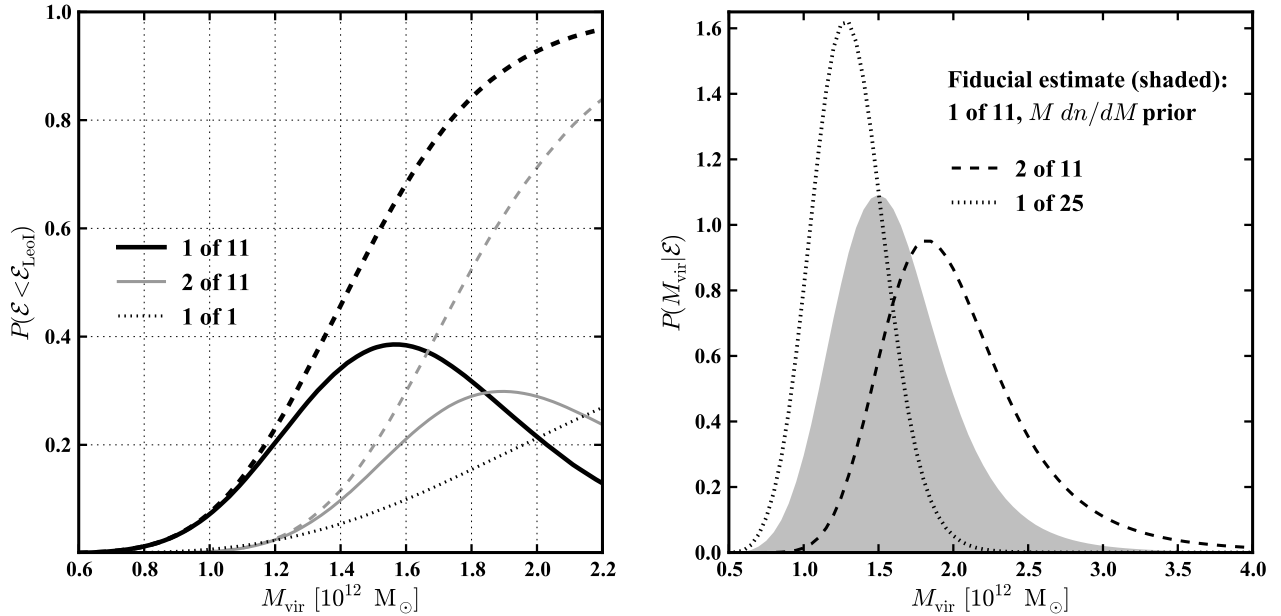


FIG. 3.— *Left*: Probability of finding N galaxies less bound than Leo I as a function of the Milky Way virial mass M_{vir} when choosing among M galaxies with well-known energies. $(N, M) = (1, 1)$ is the probability of an individual galaxy being less bound than Leo I (dotted curve), while $(1, 11)$ [solid black curve] and $(2, 11)$ [solid gray curve] correspond to finding one or two such galaxies out of a sample of eleven. Dashed curves show the probability of having *at least* 1 (black) or 2 (gray) galaxies as energetic as Leo I. *Right*: Posterior probability distribution (PPD) of the Milky Way’s virial mass for various assumptions about sample size and prior. Our fiducial case (shaded) is the estimate we consider most reliable, with Leo I being the most energetic of a sample of eleven satellite galaxies and adopting a prior for the virial mass based on the mass-weighted dark matter halo mass function. In this case, the median value of the PPD is $M_{\text{vir}} = 1.6 \times 10^{12} M_{\odot}$, with a 90% confidence interval of $M_{\text{vir}, \text{MW}} \in [1.0, 2.4] \times 10^{12} M_{\odot}$. If we instead assume that one additional MW satellite is more energetic than Leo I, we obtain a PPD given by the dashed curve, which is shifted to higher values of $M_{\text{vir}, \text{MW}}$. The dotted curve shows the PPD for the case where Leo I is the most energetic of 25 satellites (the approximate number of known Milky Way satellite galaxies). Each of these PPDs assumes a prior that is proportional to the mass-weighted dark matter halo mass function, $M_{\text{vir}} dn/dM_{\text{vir}}$. A robust result of our analysis is that $M_{\text{vir}, \text{MW}} > 10^{12} M_{\odot}$ at 95% confidence when considering the eleven classical satellites of the Milky Way, irrespective of the unknown tangential velocities of some of these satellites and of the choice of prior.

The lack of strongly constraining proper motion data for 6 of the 11 classical satellites means that, in principle, there could be as many as 6 additional satellites on orbits as energetic as Leo I. We can estimate how likely this is on a satellite-by-satellite case by comparing to the simulations by first selecting subhalos with similar Galactocentric distance and observed radial velocity for a given satellite, then using the distribution of space velocities of these subhalos to compute the distribution of orbital energies. This allows us to estimate the probability that a given satellite is on an orbit more energetic than Leo I. This probability is very low – less than 1% – in each case. Among the five satellites with well-measured space velocities, Leo I has the smallest binding energy. We note that using the measurements of Kallivayalil et al. (2006b), the LMC would have a binding energy that is comparable to, or even less than, that of Leo I. However, the revised value of the LMC’s Galactocentric velocity (Kallivayalil et al. 2012, submitted) places it on an orbit that is more bound than Leo I so long as $M_{\text{vir}, \text{MW}} \gtrsim 7 \times 10^{11} M_{\odot}$. We therefore take the scenario in which Leo I is the least bound of the eleven classical satellites as our fiducial case.

The solid black curve in the left panel of Figure 3 shows the probability of precisely one subhalo from a randomly-selected sample of eleven subhalos having a binding energy equal to or less than that of Leo I. For comparison, we also show the probability of finding precisely two galaxies from such a sample (solid gray curve). If we ask instead how often at least one subhalo has a

binding energy equal to or less than that of Leo I, we obtain the dashed black curve in left panel Figure 3. This figure shows that Leo I’s measured space velocity argues against a low mass for the Milky Way (i.e., against $M_{\text{vir}, \text{MW}} \lesssim 10^{12} M_{\odot}$). It is vanishingly rare for a randomly-chosen subhalo to be as energetic as Leo I if $M_{\text{vir}, \text{MW}} < 10^{12} M_{\odot}$, and there is less than a 10% chance of finding at least 1 such subhalo when selecting a random sample of 11 from hosts with $M_{\text{vir}, \text{MW}} < 10^{12} M_{\odot}$.

While the left panel of Figure 3 shows the likelihood of finding subhalo(s) less bound than Leo I in a halo with a given M_{vir} , a potentially more interesting quantity is the posterior probability distribution of M_{vir} given Leo I’s orbital energy, $P(M_{\text{vir}} | \mathcal{E})$. This can be easily calculated using Bayes’ theorem by combining the results of the left panel of Figure 3 with the prior probability distribution $P(M_{\text{vir}})$ for the Milky Way mass. One natural choice of prior in Λ CDM is $P(M_{\text{vir}}) = dn/dM_{\text{vir}}$, i.e., the probability of a given halo mass is proportional to the halo mass function. Another logical Λ CDM-based prior is $P(M_{\text{vir}}) = M_{\text{vir}} dn/dM_{\text{vir}}$, which approximates a stellar mass weighting¹⁵. We also consider a flat prior on M_{vir} , $P(M_{\text{vir}}) = \text{constant}$. Since the mass function decreases monotonically with M_{vir} and is never shallower than $dn/dM_{\text{vir}} \propto M_{\text{vir}}^{-1.9}$ (e.g., Boylan-Kolchin et al.

¹⁵ This weighting assumes that the probability distribution of host halo masses for a randomly selected star is proportional to the halos’ stellar content, and is perhaps the most reasonable prior if the Sun can be considered a randomly-selected star.

TABLE 1
ESTIMATES OF MILKY WAY’S VIRIAL MASS (IN UNITS OF $10^{12} M_{\odot}$).

V_i prior	0 dn/dM	measured flat	measured $M dn/dM$	measured dn/dM
1 of 11	1.1 [0.7–1.6]	1.6 [1.1–2.5]	1.6 [1.0–2.4]	1.5 [1.0–2.2]
2 of 11	1.3 [1.0–2.1]	2.1 [1.4–3.4]	2.0 [1.4–3.1]	1.9 [1.3–2.8]
3 of 11	1.6 [1.1–2.7]	2.5 [1.7–4.8]	2.3 [1.6–4.1]	2.2 [1.6–3.6]
4 of 11	1.9 [1.3–3.6]	3.1 [2.0–6.8]	2.8 [1.9–5.6]	2.6 [1.8–4.6]

NOTE. — Column (1) indicates the number of satellites with binding energies as low as Leo I; in all cases, we assume the satellites are selected from a sample of eleven (the classical Milky Way satellites). Columns (2)–(5) show the median value and 90% confidence interval of the posterior probability distribution for the virial mass of the Milky Way, in units of $10^{12} M_{\odot}$. Column (2) assumes that Leo I has zero tangential velocity (3σ away from the result of Paper I), whereas columns (3)–(5) adopt the measured tangential velocity and its error distribution but use different priors on $P(M_{\text{vir}})$. When using the measured tangential velocity, we find that $M_{\text{vir,MW}} > 10^{12} M_{\odot}$ at 95% confidence, a result that is independent of the choice of prior and the unknown tangential motions of some of the classical satellites. Our best estimate of $M_{\text{vir,MW}}$ assumes that Leo I is the most energetic classical satellite and uses a mass prior that is proportional to the mass-weighted dark matter halo mass function (row one, column four), giving a median value of $M_{\text{vir,MW}} = 1.6 \times 10^{12} M_{\odot}$.

2009), the priors incorporating the mass function assign higher weights to low-mass halos than to those with high mass and will result in lower estimates of M_{vir} than the flat prior.

The results of these calculations are presented in Table 1 and plotted in the right panel of Figure 3. We take as our fiducial estimate the case where Leo I is the most energetic galaxy out of the sample of the 11 classical Milky Way satellites with a prior of $M_{\text{vir}} dn/dM_{\text{vir}}$; this results in a posterior probability distribution (PPD) for the Milky Way’s virial mass with a median value of $1.6 \times 10^{12} M_{\odot}$ and a symmetric 90% confidence interval of $M_{\text{vir,MW}} \in [1.0, 2.4] \times 10^{12} M_{\odot}$. The PPD for this choice is plotted as the shaded gray region in the right panel of Figure 3. The median and 90% confidence interval of the PPD shift to larger values as the number of satellites as energetic as Leo I is allowed to increase: if one of the classical satellites is less bound than Leo I, then our fiducial estimates would change to $M_{\text{vir,MW}} = 1.9 \times 10^{12} M_{\odot}$ and $M_{\text{vir,MW}} \in [1.4, 3.1] \times 10^{12} M_{\odot}$ at 90% confidence. The choice of prior has a weaker effect, as can be seen from comparing values in a given row of Table 1. Even the effect of sampling from a larger number of galaxies is modest: even if we assume that *all* 25 known Milky Way dwarfs had measured proper motions and that Leo I was still the most energetic from this entire set, the median of the PPD would only decrease to $1.3 \times 10^{12} M_{\odot}$ with a 90% confidence interval of $M_{\text{vir,MW}} \in [0.9, 1.7] \times 10^{12} M_{\odot}$ for our fiducial prior.

While median and upper limits of the PPD vary based on the choice of input parameters, Table 1 shows that *the data constrain (at 95% confidence) the Milky Way mass to exceed $10^{12} M_{\odot}$, independent of prior or number of additional fast-moving satellites*. This is the strongest and most robust constraint provided by the combination of numerical simulations and the Leo I proper motion measurement. Indeed, even if we assume that Leo I has *no* tangential motion, which is ruled out at 3σ by the

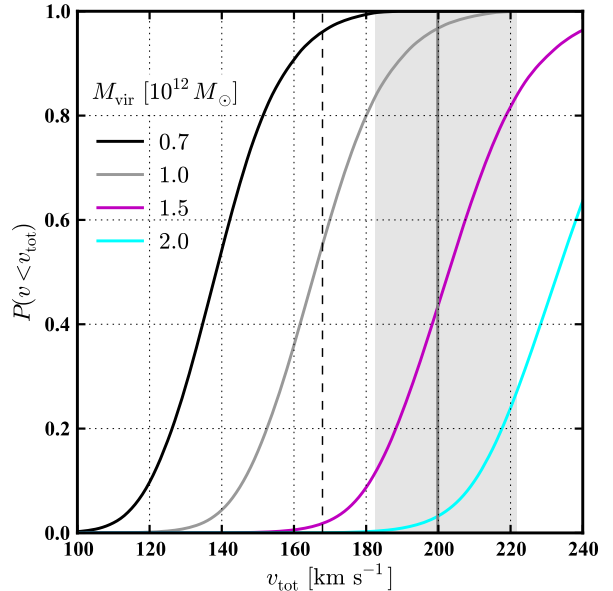


FIG. 4.— The probability that, when choosing from eleven subhalos, the most energetic will have a total velocity less than v_{tot} at D_{LeoI} . The probabilities are plotted for four values of $M_{\text{vir,MW}}/10^{12} M_{\odot}$: 0.7 (black), 1.0 (gray), 1.5 (magenta), and 2.0 (cyan). The dashed black vertical line shows the measured V_r of Leo I (which is an absolute lower limit for V_{LeoI}), while the solid gray vertical line and gray shaded region show Leo I’s measured V_{tot} and the 68.3% confidence interval about this measurement. It is very unlikely to find the fastest-moving subhalo to have V_{tot} as high as Leo I unless $M_{\text{vir,MW}} > 10^{12} M_{\odot}$.

observations of Paper I, we still find that the median of the PPD for $M_{\text{vir,MW}}$ exceeds $10^{12} M_{\odot}$ (see column 2 of Table 1).

The results of Figure 3 can also be expressed in terms of the probability of observing an object with the velocity of Leo I for different values of $M_{\text{vir,MW}}$; this is perhaps more intuitive, as it corresponds to the observed quantities. In Figure 4, we plot the probability that the most energetic subhalo out of a sample of 11 subhalos has a velocity (at D_{LeoI}) less than V , as a function of V , for four different values of $M_{\text{vir,MW}}$. The observed radial velocity of Leo I is shown as a dashed black vertical line, while the observed total velocity of Leo I is shown as a solid gray vertical line; the shaded gray region shows the 68% confidence interval about V_{tot} . The $7 \times 10^{11} M_{\odot}$ Milky Way is ruled out at 95% confidence level by the radial velocity alone (see also Table 1); including the observed tangential velocity only strengthens this conclusion. In general, it is unlikely to find the most energetic satellite (from a sample of 11) moving at Leo I’s velocity unless $1 \lesssim M_{\text{vir,MW}}/10^{12} M_{\odot} \lesssim 2$.

5. LEO I AND THE NATURE OF SATELLITE INFALL

As discussed in the Introduction, we expect to find a relationship between a satellite’s orbital energy and the time it was accreted onto its host. The existence of such a correlation could aid in a broader interpretation of Leo I’s space velocity by constraining when Leo I fell into the Milky Way and whether or not it has made multiple pericentric passages.

We explore the relationship between infall time and orbital energy in Figure 5, which shows a version of the

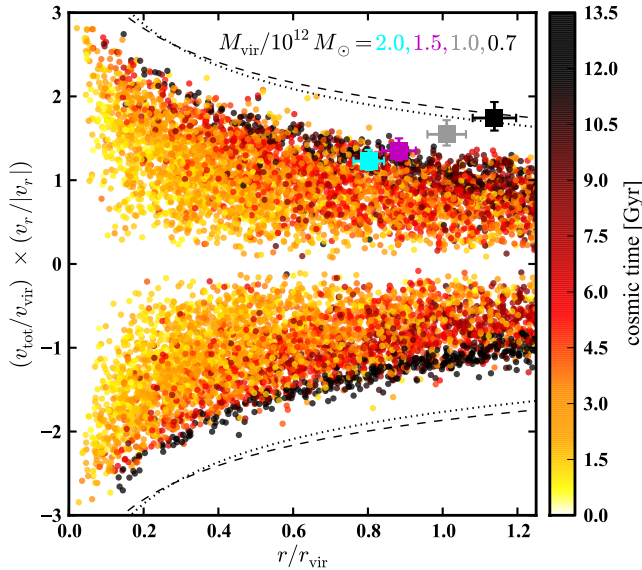


FIG. 5.— Similar to Figure 2, except each subhalo is colored according to its infall time (cosmic time, in Gyr). Subhalos that fell in long ago (yellow-orange) exhibit a wide range of orbital energies, with the largest concentration of points at small radii and high binding energies. Recently accreted subhalos (dark red-black) occupy a much narrower range of orbital energies and are substantially less bound than the typical early-infalling subhalo.

total velocity phase space for Aquarius subhalos in which each subhalo is colored according to its infall time (measured in cosmic time, with 13.7 Gyr being the present day). We clearly see an energy-infall time trend: while the early infalling objects (yellow-orange) cover a wide range of orbital energies, with the majority of subhalos being tightly bound and having apocenters of $0.75 r_{\text{vir}}$ or less, recently accreted subhalos (dark red-black) lie in a well-defined, narrow range of energies with corresponding apocenters of $\approx 2 r_{\text{vir}}$.

Recently accreted subhalos track a curve of constant energy – corresponding to $v_{\text{tot}}(r_{\text{vir}}) \approx 1.15 V_{\text{vir}}$ – quite well, especially before they reach their first pericenters. This is fully consistent with the findings of previous Λ CDM-based analyses: Wetzell (2011) finds that the typical infall velocity of satellites for hosts of $M_{\text{vir}} \approx 10^{12} M_{\odot}$ is $1.1 - 1.15 V_{\text{vir}}$ (see also Benson 2005 and Khochfar & Burkert 2006; the excellent agreement of $v_{\text{tot}}(r_{\text{vir}})$ may be partially coincidental, however, as our definition of binding energy and virial velocity differ slightly from those of Wetzell). Figure 5 supports the orbit calculations of Paper I, which strongly favor the scenario in which Leo I fell into the MW within the last ~ 2 Gyr and has recently completed its first pericentric passage (see also Rocha et al. 2012). As noted in Paper I, this orbital history agrees very well with the observed star formation history of Leo I, which shows continuous star formation until $\lesssim 1$ Gyr ago, with enhancements at 4.5 and 2 Gyr in the past, after which star formation ceased completely (T. Smecker-Hane et al., in preparation).

The confinement of first infall orbits to a narrow range of orbital energies shows how valuable measurements of transverse velocities can be for interpreting satellite dynamics. We further emphasize this point in Figure 6 by focusing only on recently accreted subhalos and contrast-

ing the resulting phase space using 3D velocities (left panel) with the phase space using only radial velocity information (right panel). The contrast is stark: while recently accreted subhalos occupy a well-defined and narrow range of the 3D phase space, these satellites cover a wide range of radial velocities at every radius. Transverse velocities clearly add a great deal of information that is missing in the radial phase space. This also implies that subhalos are typically accreted with non-negligible angular momentum, and that radial orbit approximations result in substantial information loss. A further important point is that there are recently-accreted satellites with small radial velocities but high tangential velocities, indicating that other Milky Way satellites may have binding energies similar to Leo I even if they have small measured radial velocities.

The apocentric distance for galaxies with binding energies consistent with that of Leo I in a halo of $M_{\text{vir}} = 1.6 \times 10^{12} M_{\odot}$ is ~ 650 kpc, comparable to the estimate of Peebles et al. (2011). The virial radius of such a halo is ~ 300 kpc, meaning this apocentric distance is similar to the turn-around radius (Mamon et al. 2004). The first apocenter of an orbit after turn-around is expected to be at $\sim 90\%$ of the turn-around radius in the SSIM (Bertschinger 1985; Ludlow et al. 2009), so this large apocenter value is consistent with theoretical expectations for a galaxy on its first infall.

The results of Section 5 have interesting implications for satellites on first infall into their host galaxies: Figure 5 shows that such satellites should populate a narrow range of energies. For a measured distance and radial velocity of a satellite, then, the only uncertainties are the halo mass and transverse velocity. Leo T provides just such an example for the Milky Way: a distant satellite ($D = 407$ kpc) with a low radial velocity ($v_r = -61 \text{ km s}^{-1}$ in the Galacto-centric frame), Leo T is the only known dwarf spheroidal / transition object near the Milky Way with substantial HI gas content, and is therefore almost certainly falling into the Milky Way for the first time. Our best-fitting virial mass of $1.6 \times 10^{12} M_{\odot}$ leads to a prediction for the transverse velocity of Leo T of $v_t \approx 120 \pm 20 \text{ km s}^{-1}$, i.e., Leo T’s transverse velocity should be approximately two times larger than its measured radial velocity. Future measurements of Leo T’s proper motion with *HST* (Program GO-12914; PI: T. Do) will verify or disprove this prediction. Proper motion measurements for other distant satellites such as Leo II ($D = 235$ kpc) and Canes Venatici I ($D = 218$ kpc) would also be of great interest.¹⁶

6. DISCUSSION

While the radial velocity of Leo I has been the basis of a substantial body of work related to the mass of the Milky Way and the properties of its satellites, our measurement of the proper motion of Leo I (in Paper I) adds vital information about Leo I’s orbit. We have shown that it is *a priori* extremely unlikely for Leo I to be unbound to the Milky Way in Λ CDM, as vanishingly few subhalos have velocities exceeding the local escape velocity of their host in all of the N -body simulations analyzed here.

¹⁶ Lépine et al. (2011) measured a transverse velocity of $265.2 \pm 129.4 \text{ km s}^{-1}$ for Leo II; the central value is tantalizingly large, but is also consistent with zero at 2σ .

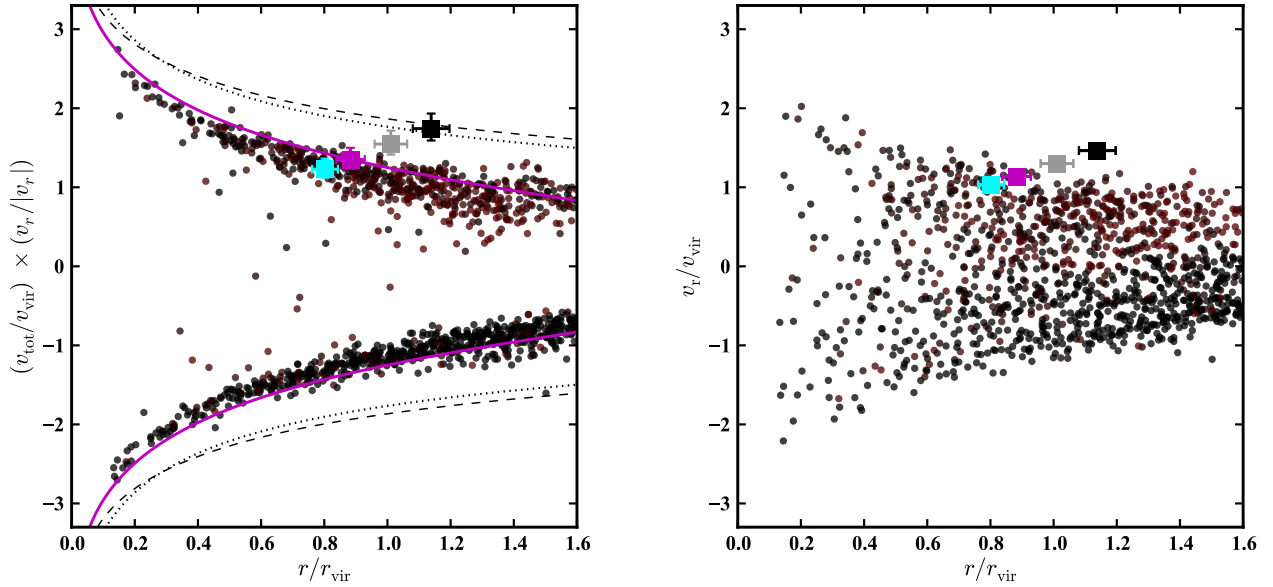


FIG. 6.— Phase space plots in terms of total velocity (left panel) and radial velocity (right panel) for subhalos accreted within the last 4 Gyr of cosmic time; the color scale is the same as in Figure 5. The curve of constant energy for an object with Leo I’s observed velocity and Galacto-centric distance in a halo of $M_{\text{vir,MW}} = 1.5 \times 10^{12} M_{\odot}$, $v_{\text{tot}}(r_{\text{vir}}) \approx 1.15 V_{\text{vir}}$, is shown in magenta. The dashed and dotted curves in the left panel are the same as in Figure 2. Whereas recently accreted satellites occupy a narrow range of velocities at fixed radius (left), they span a wide range of radial velocities (right).

By itself, this is not strongly constraining. However, we have shown that the phase space structure of subhalos in numerical simulations is very regular. We have therefore coupled the proper motion measurement with the simulations and have presented a new method for combining these data sets to derive constraints on $M_{\text{vir,MW}}$.

Our best estimate for $M_{\text{vir,MW}}$ is $1.6 \times 10^{12} M_{\odot}$ with a 90% confidence interval of $[1.0 - 2.4] \times 10^{12} M_{\odot}$. While the precise central value and upper limit of this range depend somewhat on input assumptions, our strongest finding is $M_{\text{vir,MW}} > 10^{12} M_{\odot}$ at 95% confidence, independent of mass priors or kinematic data from additional satellites. Compared to previous determinations of $M_{\text{vir,MW}}$ based on the Leo I timing argument, this best-estimate value and range are similar to Zaritsky et al. (1989) and lower than, but consistent with, Li & White (2008) and Sohn et al. (2012b). van der Marel et al. (2012b) have computed $M_{\text{vir,MW}}$ based on the timing argument for the MW-M31 pair and find an average for $M_{\text{vir,MW}}$ of $1.63 \times 10^{12} M_{\odot}$, in good agreement with our results.

Our results disfavor “light” Milky Way models, wherein $M_{\text{vir,MW}} \lesssim 10^{12} M_{\odot}$. An appealing feature of such models is that they help mitigate issues (Klypin et al. 1999; Moore et al. 1999; Boylan-Kolchin et al. 2011b, 2012) in reproducing observations of the Milky Way’s satellites in the context of Λ CDM (Wang et al. 2012; Zolotov et al. 2012; Vera-Ciro et al. 2013; Starkenburg et al. 2013). Our work, however, shows that it is extremely difficult to reproduce the observed velocity of Leo I in these low mass models. While mass constraints based on tracer stars in the Galactic halo have traditionally favored masses of $\sim 10^{12}$, we note that an NFW halo with $M_{\text{vir}} = 1.6 \times 10^{12} M_{\odot}$ and $c = 12$ has $M(< 150 \text{ kpc}) = 10^{12} M_{\odot}$, consistent with the BHB star constraint from Deason et al. (2012).

The results of this paper provide further motivation for measuring proper motions for all of the classical Galactic

satellites: Table 1 indicates that if just one more of these galaxies is found to have a binding energy as low as that of Leo I, then the 95% confidence value for the lower limit of $M_{\text{vir,MW}}$ would increase to $\approx 1.3 \times 10^{12} M_{\odot}$. Reducing the proper motion errors for Leo II is an especially high priority because the current mean value of its space motion (Lépine et al. 2011) is very large (266 km s^{-1} at a distance of 235 kpc, comparable to that of Leo I). More simulations are also needed to understand potential systematics of the method presented here. In particular, simulations of Local Group – rather than Milky Way – analogs are needed if we are to truly capture the nature of the Milky Way satellite system.

In addition to constraining the mass of the Milky Way’s dark matter halo, the orbital analysis of Paper I and the Λ CDM simulations studied here both argue for a first infall scenario in which Leo I has only recently joined the Milky Way. Coupled with (1) convincing evidence that star formation persisted in Leo I until the past 0.5–1 Gyr (Smecker-Hane et al. 2009), and (2) the lack of HI detected in Leo I ($M_{\text{HI}} < 1.5 \times 10^3 M_{\odot}$; Greveich & Putman 2009), this implies that gas in MW dwarf satellites can be either expelled or removed on time-scales shorter than one crossing time (see also Peebles et al. 2011). If the gas was expelled via internal processes, then further studies of Leo I may shed light on star formation feedback. If the gas has been removed by ram pressure, Leo I may provide an interesting constraint on the density of hot gas in the Milky Way halo.

A further implication of a recent Leo I infall, in conjunction with evidence that both Magellanic Clouds are also on their first infall (Besla et al. 2007; Boylan-Kolchin et al. 2011a), is that the Milky Way system is a dynamic one, with substantial late-time assembly. This active recent history at the dark matter halo level may initially seem odd in the context of the implied quiescent merger history for the Milky Way galaxy; however, it may simply

reflect that the Galaxy's quiescent merger history over the past several Gyr is coming to an end. The Milky Way-M31 orbit, as inferred from recent measurement of M31's proper motion (Sohn et al. 2012a; van der Marel et al. 2012a), ensures that the Milky Way's quiescent history has a maximum future duration of ~ 4 Gyr.

ACKNOWLEDGMENTS

We have enjoyed fruitful discussions with Frank van den Bosch, Alis Deason, Arianna Di Cintio, Michael Kuhlen, Aaron Ludlow, and Tammy Smecker-Hane. We thank the anonymous referee for helpful suggestions that led to improvements in the paper. The Aquarius Project is part of the program of the Virgo Consortium for cosmological simulations. We gratefully acknowledge the Aquarius, Via Lactea II, and GHALO collaborations for giving us access to their simulation data, and we thank Michael Kuhlen for providing us with a subhalo catalog

from the GHALO simulation and Mark Vogelsberger for providing the peculiar potential data for the Aquarius A halo. MB-K thanks the Kavli Institute for Theoretical Physics and the organizers of the "First Galaxies and Faint Dwarfs" workshop for providing a stimulating environment during the development of this paper and acknowledges support from the Southern California Center for Galaxy Evolution, a multi-campus research program funded by the University of California Office of Research. GB acknowledges support from NASA through Hubble Fellowship grant HST-HF-51284.01-A. This work was supported in part by the National Science Foundation under grants AST-1009973 and PHY11-25915. Support for this work was also provided by NASA through a grant for program GO-12270 from the Space Telescope Science Institute (STScI), which is operated by the Association of Universities for Research in Astronomy (AURA), Inc., under NASA contract NAS5-26555. This research has made use of NASA's Astrophysics Data System.

REFERENCES

- Anderson, M. E., & Bregman, J. N. 2010, *ApJ*, 714, 320
 Ascasibar, Y., Hoffman, Y., & Gottlöber, S. 2007, *MNRAS*, 376, 393
 Battaglia, G. et al. 2005, *MNRAS*, 364, 433
 Behroozi, P. S., Wechsler, R. H., & Conroy, C. 2012, arXiv:1207.6105 [astro-ph]
 Benson, A. J. 2005, *MNRAS*, 358, 551
 Bertschinger, E. 1985, *ApJS*, 58, 39
 Besla, G., Kallivayalil, N., Hernquist, L., Robertson, B., Cox, T. J., van der Marel, R. P., & Alcock, C. 2007, *ApJ*, 668, 949
 Boylan-Kolchin, M., Besla, G., & Hernquist, L. 2011a, *MNRAS*, 414, 1560
 Boylan-Kolchin, M., Bullock, J. S., & Kaplinghat, M. 2011b, *MNRAS*, 415, L40
 —. 2012, *MNRAS*, 422, 1203
 Boylan-Kolchin, M., Springel, V., White, S. D. M., & Jenkins, A. 2010, *MNRAS*, 406, 896
 Boylan-Kolchin, M., Springel, V., White, S. D. M., Jenkins, A., & Lemson, G. 2009, *MNRAS*, 398, 1150
 Bryan, G. L., & Norman, M. L. 1998, *ApJ*, 495, 80
 Bullock, J. S., Kolatt, T. S., Sigad, Y., Somerville, R. S., Kravtsov, A. V., Klypin, A. A., Primack, J. R., & Dekel, A. 2001, *MNRAS*, 321, 559
 Busha, M. T., Marshall, P. J., Wechsler, R. H., Klypin, A., & Primack, J. 2011, *ApJ*, 743, 40
 Byrd, G., Valtonen, M., McCall, M., & Innanen, K. 1994, *AJ*, 107, 2055
 Conroy, C., Wechsler, R. H., & Kravtsov, A. V. 2006, *ApJ*, 647, 201
 Deason, A. J. et al. 2012, *MNRAS*, 425, 2840
 —. 2011, *MNRAS*, 415, 2607
 Dehnen, W., McLaughlin, D. E., & Sachania, J. 2006, *MNRAS*, 369, 1688
 Di Cintio, A., Knebe, A., Libeskind, N. I., Hoffman, Y., Yepes, G., & Gottlöber, S. 2012, *MNRAS*, 423, 1883
 Diemand, J., & Kuhlen, M. 2008, *ApJ*, 680, L25
 Diemand, J., Kuhlen, M., & Madau, P. 2007a, *ApJ*, 657, 262
 —. 2007b, *ApJ*, 667, 859
 Diemand, J., Kuhlen, M., Madau, P., Zemp, M., Moore, B., Potter, D., & Stadel, J. 2008, *Nature*, 454, 735
 Diemer, B., More, S., & Kravtsov, A. 2012, arXiv:1207.0816 [astro-ph]
 Dutton, A. A., Conroy, C., van den Bosch, F. C., Prada, F., & More, S. 2010, *MNRAS*, 407, 2
 Fang, T., Bullock, J., & Boylan-Kolchin, M. 2013, *ApJ*, 762, 20
 Fich, M., & Tremaine, S. 1991, *ARA&A*, 29, 409
 Fillmore, J. A., & Goldreich, P. 1984, *ApJ*, 281, 1
 Flynn, C., Holmberg, J., Portinari, L., Fuchs, B., & Jahreiß, H. 2006, *MNRAS*, 372, 1149
 Fukugita, M., & Peebles, P. J. E. 2004, *ApJ*, 616, 643
 Ghigna, S., Moore, B., Governato, F., Lake, G., Quinn, T., & Stadel, J. 1998, *MNRAS*, 300, 146
 Gill, S. P. D., Knebe, A., & Gibson, B. K. 2005, *MNRAS*, 356, 1327
 Gnedin, O. Y., Brown, W. R., Geller, M. J., & Kenyon, S. J. 2010, *ApJ*, 720, L108
 Grevecich, J., & Putman, M. E. 2009, *ApJ*, 696, 385
 Gunn, J. E., & Gott, J. R. I. 1972, *ApJ*, 176, 1
 Guo, Q., White, S., Li, C., & Boylan-Kolchin, M. 2010, *MNRAS*, 404, 1111
 Gupta, A., Mathur, S., Krongold, Y., Nicastro, F., & Galeazzi, M. 2012, *ApJ*, 756, L8
 Hayashi, E., Navarro, J. F., & Springel, V. 2007, *MNRAS*, 377, 50
 Kahn, F. D., & Woltjer, L. 1959, *ApJ*, 130, 705
 Kallivayalil, N., van der Marel, R. P., & Alcock, C. 2006a, *ApJ*, 652, 1213
 Kallivayalil, N., van der Marel, R. P., Alcock, C., Axelrod, T., Cook, K. H., Drake, A. J., & Geha, M. 2006b, *ApJ*, 638, 772
 Khochfar, S., & Burkert, A. 2006, *A&A*, 445, 403
 Klypin, A., Kravtsov, A. V., Valenzuela, O., & Prada, F. 1999, *ApJ*, 522, 82
 Klypin, A., Zhao, H., & Somerville, R. S. 2002, *ApJ*, 573, 597
 Klypin, A. A., Trujillo-Gomez, S., & Primack, J. 2011, *ApJ*, 740, 102
 Knebe, A., Libeskind, N. I., Doumler, T., Yepes, G., Gottlöber, S., & Hoffman, Y. 2011, *MNRAS*, 417, L56
 Knollmann, S. R., & Knebe, A. 2009, *ApJS*, 182, 608
 Kochanek, C. S. 1996, *ApJ*, 457, 228
 Komatsu, E. et al. 2011, *ApJS*, 192, 18
 Kravtsov, A. V., Gnedin, O. Y., & Klypin, A. A. 2004, *ApJ*, 609, 482
 Lépine, S., Koch, A., Rich, R. M., & Kuijken, K. 2011, *ApJ*, 741, 100
 Li, Y.-S., & White, S. D. M. 2008, *MNRAS*, 384, 1459
 Ludlow, A. D., Navarro, J. F., Springel, V., Jenkins, A., Frenk, C. S., & Helmi, A. 2009, *ApJ*, 692, 931
 Macciò, A. V., Dutton, A. A., van den Bosch, F. C., Moore, B., Potter, D., & Stadel, J. 2007, *MNRAS*, 378, 55
 Mamon, G. A., Sanchis, T., Salvador-Solé, E., & Solanes, J. M. 2004, *A&A*, 414, 445
 Mateo, M., Olszewski, E. W., & Walker, M. G. 2008, *ApJ*, 675, 201
 Mateo, M. L. 1998, *ARA&A*, 36, 435
 McConnachie, A. W. 2012, *AJ*, 144, 4
 McMillan, P. J. 2011, *MNRAS*, 414, 2446
 Moore, B., Ghigna, S., Governato, F., Lake, G., Quinn, T., Stadel, J., & Tozzi, P. 1999, *ApJ*, 524, L19
 Moster, B. P., Naab, T., & White, S. D. M. 2013, *MNRAS*, 428, 3121
 Navarro, J. F., Frenk, C. S., & White, S. D. M. 1997, *ApJ*, 490, 493

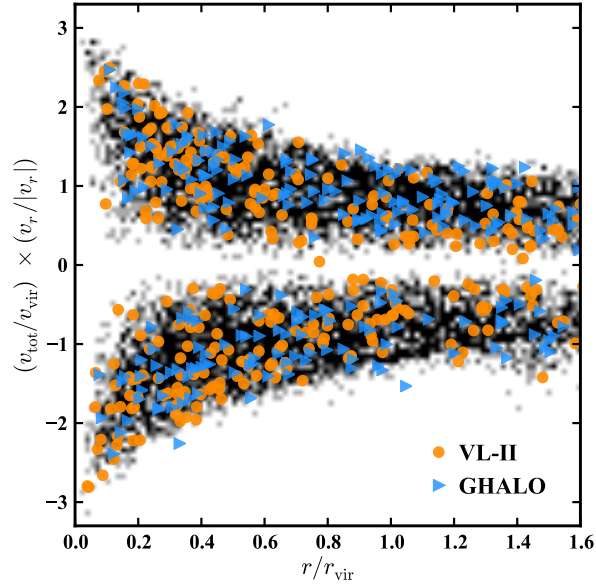


FIG. 7.— Same as Fig. 2, but also including simulations with WMAP3 parameters (VL-II: orange circles; GHALO: blue triangles). Subhalos from these simulations populate the phase space diagram in an identical manner to the Aquarius subhalos; our Aquarius-based results should therefore be robust to modest changes in cosmological parameters. Note that VL-II has a mass of $M_{\text{vir}} = 1.7 \times 10^{12} M_{\odot}$, which is near the upper end of the Aquarius halo masses, while GHALO has $M_{\text{vir}} = 1.08 \times 10^{12} M_{\odot}$, which is near the lower end. The virial scalings used throughout this work appear to be appropriate.

- Navarro, J. F. et al. 2010, MNRAS, 402, 21
Peebles, P. J. E., Tully, R. B., & Shaya, E. J. 2011, arXiv:1105.5596 [astro-ph]
Piatek, S., Pryor, C., Bristow, P., Olszewski, E. W., Harris, H. C., Mateo, M., Minniti, D., & Tinney, C. G. 2006, AJ, 131, 1445
—, 2007, AJ, 133, 818
Piatek, S., Pryor, C., & Olszewski, E. W. 2008, AJ, 135, 1024
Reddick, R. M., Wechsler, R. H., Tinker, J. L., & Behroozi, P. S. 2012, arXiv:1207.2160 [astro-ph]
Reyes, R., Mandelbaum, R., Gunn, J. E., Pizagno, J., & Lackner, C. N. 2011, MNRAS, 417, 2347
Rocha, M., Peter, A. H. G., & Bullock, J. 2012, MNRAS, 425, 231
Sales, L. V., Navarro, J. F., Abadi, M. G., & Steinmetz, M. 2007, MNRAS, 379, 1475
Schönrich, R. 2012, MNRAS, 427, 274
Smecker-Hane, T. A., Marsteller, B., Cole, A., Bullock, J., & Gallagher, J. S. 2009, in Bulletin of the American Astronomical Society, Vol. 41, #419.11
Smith, M. C. et al. 2007, MNRAS, 379, 755
Sohn, S. T., Anderson, J., & van der Marel, R. P. 2012a, ApJ, 753, 7
Sohn, S. T., Besla, G., van der Marel, R. P., Boylan-Kolchin, M., Majewski, S. R., & Bullock, J. S. 2012b, arXiv:1210.6039 [astro-ph]
Sohn, S. T. et al. 2007, ApJ, 663, 960
Springel, V. et al. 2008a, MNRAS, 391, 1685
—, 2008b, Nature, 456, 73
Stadel, J., Potter, D., Moore, B., Diemand, J., Madau, P., Zemp, M., Kuhlen, M., & Quilis, V. 2009, MNRAS, 398, L21
Starkenburg, E. et al. 2013, MNRAS, 429, 725
Teyssier, M., Johnston, K. V., & Kuhlen, M. 2012, MNRAS, 426, 1808
van der Marel, R. P., Besla, G., Cox, T. J., Sohn, S. T., & Anderson, J. 2012a, ApJ, 753, 9
van der Marel, R. P., Fardal, M., Besla, G., Beaton, R. L., Sohn, S. T., Anderson, J., Brown, T., & Guhathakurta, P. 2012b, ApJ, 753, 8
Vera-Ciro, C. A., Helmi, A., Starkenburg, E., & Breddels, M. A. 2013, MNRAS, 428, 1696
Wang, H., Mo, H. J., & Jing, Y. P. 2009, MNRAS, 396, 2249
Wang, J., Frenk, C. S., Navarro, J. F., Gao, L., & Sawala, T. 2012, MNRAS, 424, 2715
Watkins, L. L., Evans, N. W., & An, J. H. 2010, MNRAS, 406, 264
Wetzel, A. R. 2011, MNRAS, 412, 49
Xue, X. X. et al. 2008, ApJ, 684, 1143
Yang, X., Mo, H. J., van den Bosch, F. C., Zhang, Y., & Han, J. 2012, ApJ, 752, 41
Zaritsky, D., Olszewski, E. W., Schommer, R. A., Peterson, R. C., & Aaronson, M. 1989, ApJ, 345, 759
Zolotov, A. et al. 2012, ApJ, 761, 71

APPENDIX

COSMOLOGICAL PARAMETER (IN)DEPENDENCE

A possible concern in interpreting the orbit of Leo I through the use of the Aquarius simulations is that the cosmological parameters adopted for Aquarius differ slightly from the currently favored values. Specifically, WMAP7 results indicate that $\sigma_8 = 0.816 \pm 0.024$, $\Omega_m = 0.274 \pm 0.011$, and $n_s = 0.968 \pm 0.012$ (Komatsu et al. 2011), placing the Aquarius parameters 3-10% off of the most recently measured values. To investigate the effects of variations in cosmological parameters, Figure 7 duplicates Figure 2 but also includes data for subhalos from two simulations using WMAP3 parameters ($\Omega_m = 0.237$, $\sigma_8 = 0.742$, $n_s = 0.951$): VL-II (orange circles) and GHALO (blue triangles). Together, first and third-year WMAP parameters bracket parameters determined from the seven-year WMAP data release. The subhalos from WMAP3-based simulations populate phase space identically to those from the Aquarius simulations, indicating that small changes to cosmological parameters will have no effect on interpretations of Leo I's motion.